

Thermal Responses of the Properties of Cathode and Anode during Hydrogen Production and Performance of Reversible Solid Oxide Cell

Jai-Houng Leu,^{1*} Ay Su,^{2**} Shun-Chi Kuo,³
Li-Hsing Fang,⁴ Kuang-Chung Chen,¹ and Tian-Syung Lan⁵

¹School of Computer Science, Weifang University of Science and Technology,
Weifang City, Shandong Province, China

²Distinguish Professor, National Yunlin University, Yunlin County 32003, Taiwan, R.O.C.

³Department of Mechanical and Industrial Engineering, Vanung University,
Taoyuan City 32003, Taiwan, R.O.C.

⁴Department of Mechanical Engineering, Nanya Institute of Technology,
No. 414, Section 3, Zhongshan E Rd., Zhongli District, Taoyuan City 320, Taiwan

⁵Department of Information Management, Yu-Da University of Science and Technology,
Miaoli County, Taiwan, R.O.C.

(Received January 27, 2025; accepted May 26, 2025)

Keywords: electrode porosity, average pore size, temperature gradient, simulation, convection, RSOC

The performance of a reversible solid oxide cell (RSOC) was simulated considering the properties of the cathode and anode materials, such as porosity, permeability, and operating temperature. Simulation results showed that the temperature distributions in the cathode and anode differ because of their contrasting thermal responses. The performance of the fuel cell was improved at high temperature, porosity, and permeability. However, excessive heat caused thermal expansion. Therefore, the cathode and anode materials of the fuel cell must be selected to maintain optimal operating temperature, porosity, and permeability as they affect hydrogen production and overall performance. The conductivity of electrode materials decreases with increasing temperature, and the conduction mechanism is similar to that of metallic conductivity. During the operation of an oxide fuel cell (SOFC), as the temperature rises and falls, the different thermal expansion coefficients of the electrolyte and cathode materials cause peeling and cracking, which can lead to a reduction in battery performance. Because of the correlation between the production temperature and the amount of chlorine produced by hydrogen, the application of sensors that can measure both the temperature and the hydrogen concentration is an important direction of development.

1. Introduction

Reversible solid oxide cells (RSOCs) have been extensively used owing to their efficient power generation and hydrogen production. As a solid oxide electrolysis cell (SOEC) and a solid

*Corresponding author: e-mail: jahonleu@yahoo.com.tw

**Corresponding author: e-mail: meaysu@saturn.yzu.edu.tw

<https://doi.org/10.18494/SAM5573>

oxide fuel cell (SOFC), the efficiency of RSOCs largely depends on the operating temperature and humidity. In operation, oxygen transported through the porous cathode is reduced to oxygen ions (O_2^-) at the gas–cathode–electrolyte three-phase interface. The oxygen ion at the cathode–electrolyte interface is transported to the anode–electrolyte interface through the ion-conducting electrolyte. At the same time, fuel transported from the fuel channel through the porous anode to the anode–electrolyte interface is oxidized electrochemically at the three-phase interface. The products (H_2O and CO_2) are then transported back to the fuel channel through the porous anode. Transport resistances of the gas species in the porous electrodes including O_2^- in the electrolyte and the activation energy barriers for electrochemical reactions result in ohmic polarization. In ohmic polarization, concentration and activation polarizations occur owing to the transport resistance of the gaseous species through porous electrodes (anode and cathode, respectively). These polarizations alter the operating conditions and the physical properties of the RSOC, including temperature, pressure, porosity, tortuosity, permeability, the thickness of the electrode, ionic conductivity, the activity of the electrode–electrolyte interface, and fuel and oxidizer concentrations.⁽¹⁾

Oxygen is reduced to oxygen ions (O^{2-}) when it is transported through the porous cathode from the air passage at the gas–cathode–electrolyte three-phase boundary. The oxygen ions formed are then transported to the anode–electrolyte interface. At the same time, the fuel (hydrogen) is delivered through a porous anode to the anode–electrolyte interface. Then, it is electrochemically oxidized into a product. The transport resistance of the gas-phase species occurred in the porous electrode and that of O^{2-} in the electrolyte. The activation energy barrier of the electrochemical reaction results in various polarizations at the same time.

By incorporating electrochemical complexity into the analysis and interpretation of scientific results, the development of new simulation methods should be accelerated and improved. The ethos of this approach coincides with Chemkin's role in homogeneous chemical modeling, including combustion. The app must have all the electrochemical CA probabilities to set the stage for future expansion. The novelty of this work is the identification of common aspects of electrochemistry that are generally applicable to wide ranges of material groups and applications.

In this study, we investigated the effects of the porosity, permeability, and operating temperature of the cathode and anode on the operating efficiency of RSOCs. The results contribute to the improvement of RSOCs and the development of sensors used in fuel cells and SOFC power management and conversion technology on the basis of the collected data from the sensors. The improvement in RSOCs allows for enhanced power supply stability and quality to reduce power generation costs.

2. Literature Review

In SOFCs, nickel–yttria-stabilized zirconia (Ni–YSZ), yttria-stabilized zirconia (YSZ), and lanthanum strontium manganite are used for the anode, electrolyte, and cathode at an operating temperature of 850 °C, and the electrolytic performance is maintained at 2.0 A/cm² at 0.6 V and 1.5 A/cm² at 1.3 V. General Electric has used strontium-containing lanthanum manganese oxide (LSM), lithium–sulfur fluoride (LSF), and lanthanum strontium cobalt ferrite (LSCF) for the

catalytic layer and cathode and obtained 1.1–2.9 A/cm² at 0.6 V for battery performance and 0.9–1.6 A/cm² at 1.3 V for electrolytic performance at 800 °C. LSF and LSCF allowed a higher efficiency than lanthanum strontium manganite as they can maintain increased ion conductivity stably for a long time.⁽²⁾ Table 1 shows the performance of SOFCs with different materials in the electrodes.

The porosity of the cathode affects the power generation more considerably than that of the anode.⁽⁵⁾ The efficiency of power generation increases with the porosity of the cathode. In contrast, it does not increase until the anode porosity reaches 0.4 on the fuel cell. Nagata *et al.* investigated the effect of the recombinants of materials. He simulated the SOFC performance and obtained the result that the power generation efficiency decreased when the reaction rate of the recombinant increased accompanied by the outlet gas temperature.⁽⁴⁾ Henriques *et al.* simulated the fuel cell performance by changing the geometry of the air–electrode runner plate. They found that air and water were generated in the electrode, reducing the efficiency of the fuel cell accompanied by a change in current density distribution.⁽⁶⁾

3. Methods

3.1 Multifield coupled finite element model

3.1.1 Overall electrochemical model

$$V = E_{Th} - \eta = E_{Th} - \eta_{act} - \eta_{ohm} - \eta_{con}$$

$$E_{Th} = V_{oc} + \frac{RT}{nF} \ln \frac{\prod a_{products}^{v_i}}{\prod a_{reactants}^{v_i}} \quad (1)$$

V : voltage; E_{Th} : thermal electrode potential; η : overpotential

η_{act} : activation overpotential; η_{ohm} : ohm overpotential; η_{con} : concentration overpotential

T : absolute zero (273.15 °C)

R : ideal gas constant

Table 1
Electrolytic performance obtained using different materials in SOFCs.

Reference	Material			Temperature (°C)	Parameter		Current density (A/cm ²)	
	Anode	Cathode	Electrolyte		Flow rate	Fuel	At 0.6 V	At 1.3 V
GE ⁽²⁾	Ni/YSZ	LSM	YSZ	800	200 sccm	50% H ₂ /50% H ₂ O	1.1	−0.9
		LSF					1.9	−1.2
		LSCF					2.9	−1.6
Risoe National Laboratory ⁽³⁾	Ni/YSZ	LSM	YSZ	750	50% H ₂ /50% H ₂ O	0.9	−0.5	
850				2		−1.5		
Kansai Electric Power Company ⁽⁴⁾	Ni/YSZ	LSM	YSZ	800	50% H ₂ /50% H ₂ O	60 m	−50 m	
900				110 m		−125 m		

F : Faraday constant (96485 C/mol)

n : number of electrons transferred in the reaction

V_{oc} : open road pressure

V_i : voltage of interface

$a_{products}$: specific surface area of product

$a_{reactants}$: specific surface area of reactant

The current generated by the battery can be estimated using the following Butler-Volmer equation:

$$j = j_0 \times \left[\exp\left(\frac{\alpha n F \eta_{act}}{RT}\right) - \exp\left(\frac{(1-\alpha) n F \eta_{act}}{RT}\right) \right], \quad (2)$$

where j is the current density of the electrode, j_0 is the exchange current density, and α is the charge transfer coefficient.

Activation overpotential, Ohm overpotential, and concentration overpotential can be deduced from the following equations:

$$\begin{aligned} \eta_{act} &= \left(\frac{RT}{n\alpha_a F}\right) \ln\left(\frac{j}{j_{0a}}\right) - \left(\frac{RT}{n\alpha_c F}\right) \ln\left(\frac{j}{j_{0c}}\right), \\ \eta_{ohm} &= jASR_{ohm}, \\ \eta_{conc} &= \frac{RT}{nF} \left(1 + \frac{1}{\alpha_i}\right), \end{aligned} \quad (3)$$

where α_a and α_c denote the dimensionless anodic and cathodic charge transfer coefficients, α_i denotes the dimensionless interface charge transfer coefficient, S is mainly used by Siemens (the unit of electric conductance, electric susceptance, and electric admittance), R_{ohm} is the resistivity, and A is the area, j_{0a} is the exchange current density of the anode, and j_{0c} is the exchange current density of the cathode.

3.1.2 Controlling equation within the porous electrode

The Stefan–Maxwell equation is used to describe the flow of fluid in this region as follows.

$$-\nabla X_i = \sum_{j=1, j \neq i}^n \frac{X_j N_i - X_i N_j}{CD_{i,j}} \quad (4)$$

Here, X_i is the mole fraction on species i , C is the total molar concentration, D_i is the diffusional driving force acting on species i , N is the mean number of the molar species transferred in the

reaction.

The open-circuit voltage (OCV) is calculated using the Nernst equation.

$$E_{ideal,H_2} = \frac{1}{2F} \left[\Delta G(T) + RT \ln \left(\frac{P_{H_2} \cdot P_{O_2}^{1/2}}{P_{H_2O}} \right) \right] \quad (5)$$

where P is the pressure and G is the conductance of the object.

The partial pressures of hydrogen and oxygen can be obtained by concentration conversion using the ideal gas equation. The same current is estimated using the Butler-Volmer equation.

$$j = j_0(T, P_i) \times \left[\exp \left(\alpha_a \frac{nF\eta_{act}}{RT} \right) - \exp \left(-\alpha_c \frac{nF\eta_{act}}{RT} \right) \right] \quad (6)$$

The mass transfer effect and ohmic impedance cannot be observed in the one- or two-dimensional model. However, the internal flow field, mass transfer, electric field, and chemical phenomena of the breathing proton exchange membrane fuel cell can be further explored in a three-dimensional model. The numerical model of this study was used to establish the 3D model shown in Fig. 1.

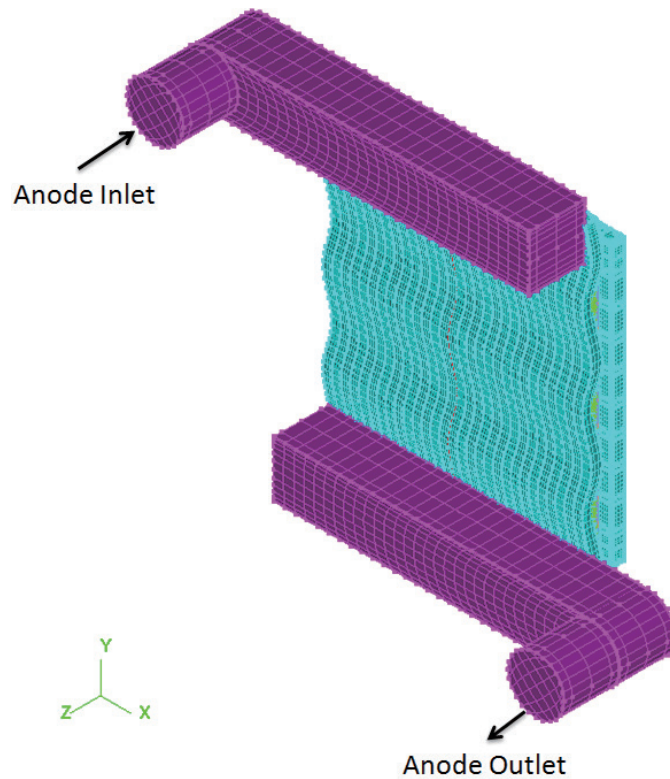


Fig. 1. (Color online) 3D simulation model of the anode.

3.2 Simulation and algorithms

The following materials, structures, and conductivity were used in this study. The conductivity of the cathode material exceeds 100 s/cm. When the conductivity of the anode reaches more than 105 s/cm, the anode reduces the difference in the coefficient of thermal expansion (CTE) between the anode and the solid electrolyte. The recommended cathode material for this reversible SOFC (RSOFC) is either strontium-containing lanthanum oxide (Sr-doped LaCoO₃, LSC) or strontium-containing lanthanum manganese oxide (Sr-doped LaMnO₃, LSM). Moreover, the anode material is a ceramic–gold material (cermet, Ni–YSZ), which is a mixture of nickel (Ni) and YSZ in appropriate proportions.

In this study, simulations were performed using the Composites Module and the COMSOL compiler™. In addition, by using the Application Builder in COMSOL Multiphysics® version 5.4, the complexity of the model simulation can be increased. There is little available data on kinetic parameters, so experiments are needed to determine the parameters. Fuel cells are seen as a closed system, making them difficult experimental targets, and many physical parameters can affect electrochemical processes. For this reason, simulations are often employed in fuel cell research, using the data obtained by electrochemical impedance spectroscopy and cyclic voltammetry.⁽²⁾ Once the kinetics are established, the electrochemical model is created. The operating voltage and current are used as inputs to simulate fuel cells of different materials.

The condensate model is used to describe the transfer of dissolved gases in the electrolyte, in addition to their transfer to the reaction site in the bipolar plate fuel cell.⁽⁷⁾ The operating temperature distribution is affected by the interface where the chemical species are transferred through the cathode and anode pores. It is assumed that the cell sizes for this study are 10 × 10 cm² and 16 × 16 cm².⁽⁸⁾ The simulation was carried out in a grid of 900 identical fuel cells. Performance characteristics at operating temperatures of 600, 700 and 800 °C are simulated. We explore the thermal response on the basis of the performance of the fuel cell according to the modulated properties of this fuel cell.

4. Results and Discussion

Before the design parameter analysis, a benchmark control group must be established in order to compare different parameters. The parameter settings of the benchmark control group are

Table 2
Simulation parameter settings of the control group.

Parameter	Cathode	Anode
Porosity	0.6	0.6
Average pore size inside electrode (μm)	1	1
Internal permeability of electrode (m ²)	1 × 10 ⁻¹²	1 × 10 ⁻¹²
Effective surface area of electrode (1/m)	1000	1000
Equivalent ratio	5	3
Operating temperature (°C)	1000	1000

shown in Table 2.

In the simulation, hydrogen was produced mainly on the cathode. The increased cathode porosity contributed to the increase in the contact area and reaction efficiency of reactants, but the effect was limited by the reaction speed (Fig. 2). The pore size had a limited effect on fuel cell performance, as shown in Fig. 3.

The simulation results indicated that cathode/anode porosity, water vapor content, and operating temperature have significant effects on the hydrogen production in the fuel cell. The pore size of the electrode has a limited impact. When the cathode porosity increased from 0.2 to 0.4 and from 0.4 to 0.6, the hydrogen production did not notably increase.

When using Ni-YSZ and LSM at 850 °C, the performance values of the fuel cell are 2.0 A/cm² (@0.6 V) and 1.5 A/cm² (@1.3 V). At 800 °C, when we change the cathode materials to

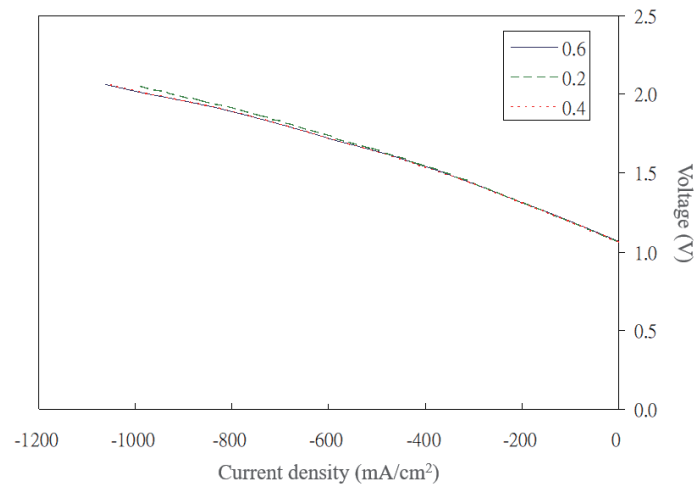


Fig. 2. (Color online) Effect of cathode porosity on fuel cell performance.

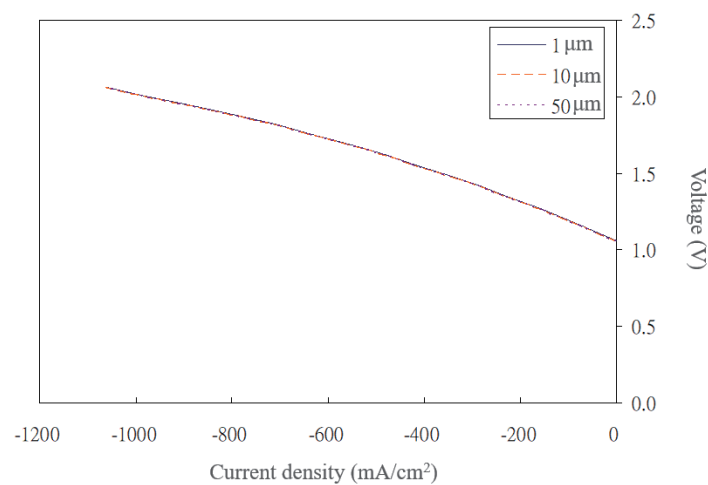


Fig. 3. (Color online) Effect of pore size of cathode on fuel cell performance.

LSM, LSF, and LSCF, the performance values of the fuel cell are 1.1, 1.9, and 2.9 A/cm² (@0.6 V), while the electrolysis performance values are 0.9, 1.2, and 1.6 A/cm² (@1.3 V), respectively. Owing to ionic conductivity, LSCF outperforms LSM, and hence, LSCF can operate stably for a longer time. The performance characteristics of LSF and LSCF are superior to those of LSM.⁽²⁾ LSCF ($\text{La}_{0.6}\text{Sr}_{0.4}\text{Co}_{0.8}\text{Fe}_{0.2}\text{O}_{3-\delta}$) has good catalytic and conductive properties. BSCF ($\text{Ba}_{0.5}\text{Sr}_{0.5}\text{Co}_{0.8}\text{Fe}_{0.2}\text{O}_{3-\delta}$) is a synthesized international oxygen-permeable membrane material widely used as an electrocatalytic material in both high- and low-temperature electrochemical reactions.

The effect of operating temperature on the performance of the fuel cell is shown in Fig. 4. With higher operating temperature, more hydrogen was produced because high temperature accelerated the chemical reaction. The temperature gradients in the upper, middle, and lower parts of the electrolyte were similar in the flow channel, but the highest temperature was observed in the middle part owing to the generation of counterflow.⁽⁹⁾

The cathode and anode showed a similar temperature distribution, which indicated that the inner part was more heated than the outer part owing to the thermal responses of the cathode and anode. The recirculation of the produced hydrogen accumulates heat owing to the counterflow effect.⁽⁹⁾ The counterflow disperses heat in the middle part of the electrode.⁽¹⁰⁾ This “heat sink mechanism” is commonly observed in the electrode of RSOCs. The performance of the RSOCs improves at higher temperatures. However, excessive heat causes a different thermal expansion of the materials. Therefore, the heat properties of materials must be considered in order to maintain high operating temperatures. The concentrations of hydrogen and oxygen were higher in the lower part of the electrode as they were forced to move down by the flow channel.⁽⁹⁾

In Fig. 5, LSCF shows high conductivity that decreases as the temperature rises. The conductivity of the LSCF + BSCF compound decreases as the temperature rises, and its conduction mechanism is similar to that of metallic conductivity. In contrast, the much lower conductivity of BSCF initially increases with temperature, but reaches a certain temperature where it exhibits a turning point and begins to decrease with increasing temperature. Many reports⁽¹¹⁾ indicate that the ideal conductivity of cathode materials must reach 100 S/cm at 800

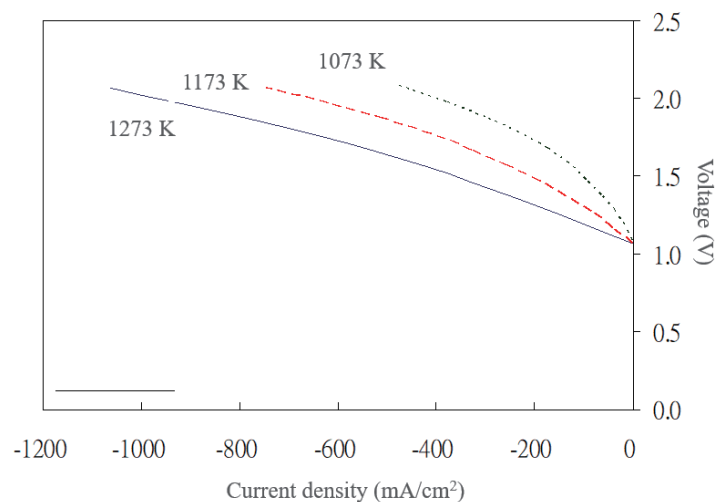


Fig. 4. (Color online) Effect of operating temperature on fuel cell performance.

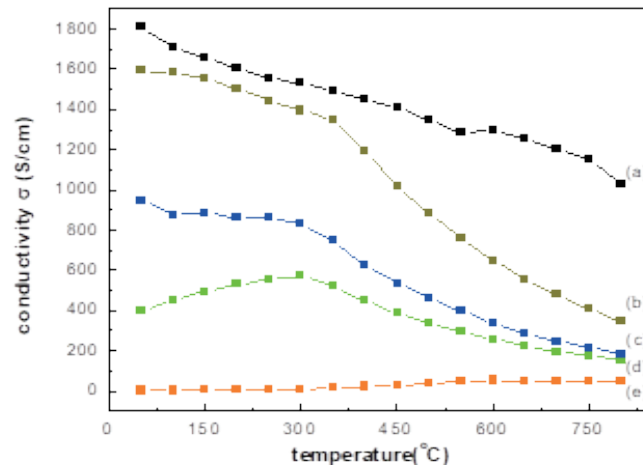


Fig. 5. (Color online) Electrical conductivity of (a) LSCF. BSCF+LSCF composite calcined at (b) 1000, (c) 1050, and (d) 1100 °C for 9 h in air. (e) BSCF.

°C, which may be the criteria for selecting the cathode material (and/or anode material).

Peters *et al.* studied anode recycling and concluded that the main driving factors for anode recycling are improved fuel efficiency and independence from external water sources during the fuel forming process. Furthermore, the impact of the anode is so minimal that it was disregarded.⁽¹²⁾ Hydrogen production is enhanced under abundant water vapor and higher operating temperatures, as the chemical reactions accelerate at high temperatures, producing more hydrogen.⁽¹²⁾

Figure 6 presents the effect of cathode permeability on RSOC performance. The performance worsens at a low permeability of the cathode as gas transfer through convection is limited inside the electrode. The materials of the fuel cell are important to its performance. The materials must be chosen to maintain high permeability and corrosion resistance to increase porosity and pore size at a high operating temperature in order to increase water vapor content.

Figure 7 shows the thermal expansion curves measured using a thermal expansion analysis instrument for a sintered body of mixed candidates after being fired at different temperatures, ranging from 50 to 1000 °C. The curves indicate an almost linear relationship with temperature increase, but an unusual thermal expansion occurs after a turning point. Therefore, it can be inferred that the second stage of abnormal thermal expansion is caused by a higher concentration of oxygen vacancies. Thermogravimetric analysis reveals that mixing results in a larger number of oxygen vacancies, causing repulsion between atoms.

Table 3 shows the calculated CTE with the overall thermal expansion coefficient ranging from 12.9 to $18 \times 10^{-6} \text{ K}^{-1}$. When compared with the oxygen defects from thermal weight loss, it can be found that the larger the number of oxygen defects, the larger the thermal expansion coefficient. This is mainly because the defects of oxygen in the lattice increase the repulsive forces between cations, leading to lattice expansion. The occurrence of the second abnormal thermal expansion coefficient is due to the maintenance of electrical neutrality, where transition

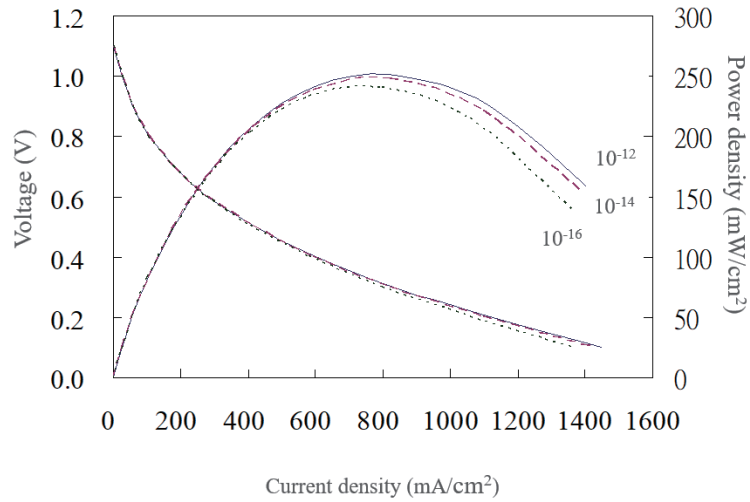


Fig. 6. (Color online) Effect of cathode permeability on RSOC performance.

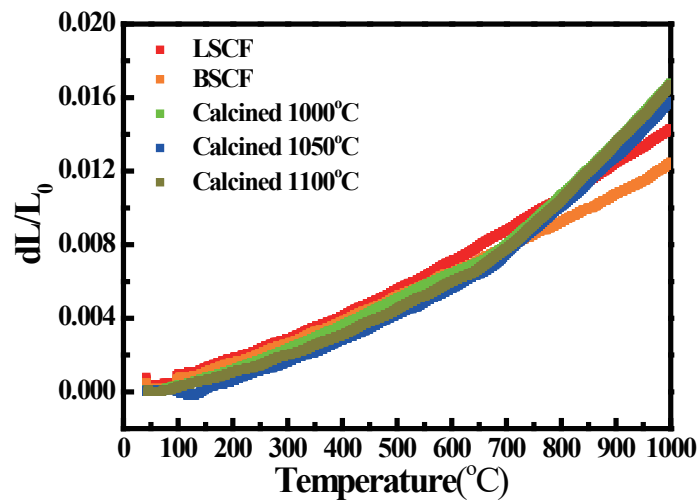


Fig. 7. (Color online) Thermal expansion curves of LSCF, BSCF, and BSCF + LSCF composite.

Table 3

Thermal expansion coefficients (TECs) of LSCF, BSCF, and BSCF + LSCF composite calcined at various temperatures.

Sample	50–400 °C ($\times 10^{-6} \text{ K}^{-1}$)	400–800 °C ($\times 10^{-6} \text{ K}^{-1}$)	50–800 °C ($\times 10^{-6} \text{ K}^{-1}$)
LSCF	12.3	18.1	14.6
BSCF	11.4	15.3	12.9
BSCF + LSCF (calcined 1000)	11.8	26.6	17.7
BSCF + LSCF (calcined 1050)	10.0	28.1	17.3
BSCF + LSCF (calcined 1100)	11.1	27.3	17.6

elements are reduced from high valence to low valence, resulting in an increase in ionic radius.

During the assembly and operation of SOFCs, a temperature increase must occur. The different thermal expansion coefficients of the electrolyte and cathode materials can lead to delamination and cracking, which result in reduced battery performance. Currently, in cathode materials, the thermal expansion coefficients are all higher than that of the electrolyte ($9\text{--}11 \times 10^{-6} \text{ K}^{-1}$). As a result, many scholars have attempted to reduce the thermal expansion coefficient of cathode materials by doping the electrolyte, or substituting cobalt with ions of higher valence or smaller radius, such as doping with nickel, iron, or copper ions, which can effectively reduce the thermal expansion coefficient.

6. Conclusions

We investigated the effects of the properties of cathode and anode materials on the performance of a fuel cell (ROSC). The porosity of the cathode has a significant impact on the power generation efficiency of the fuel cell. In contrast, the impact of the porosity of the anode can be neglected. The produced hydrogen was concentrated at the lower part of the fuel cell because of the flow channel. A high operating temperature improves the performance of the fuel cell by inducing the production of more hydrogen, but too much heat causes different expansion levels for different materials, resulting in thermal expansion. The average pore size and porosity of $1 \mu\text{m}$ and 0.2 seemed to be optimal for maintaining the function of the electrode, corrosion resistance, an appropriate operating temperature, and water vapor content. The performance of the fuel cell was worse when the permeability of the cathode was smaller. The results of this study suggested that the materials for the fuel cell electrode must be selected carefully considering the porosity and permeability in order to produce hydrogen efficiently at a high temperature and, as a result, to improve the overall performance.

LSCF has high conductivity that decreases as the temperature rises. The conductivity of the LSCF + BSCF compound decreases as the temperature rises, and its conduction mechanism is similar to that of metallic conductivity. During the assembly and operation of an SOFC, a temperature increase is required. The different thermal expansion coefficients of the electrolyte and cathode materials can lead to peeling and cracking, which can result in a decrease in battery performance.

The cathode material recommended for this RSOFC is strontium-doped lanthanum cobalt oxide (LaCoO_3 , LSC) or strontium-doped lanthanum manganite (LaMnO_3 , LSM), both of which are perovskite types. The anode material is a cermet composed of Ni and a suitable amount of YSZ.

Sensor technology also needs to be developed to accurately measure the gas temperature and maintain the optimal distribution of the produced hydrogen inside the fuel cell. Because of the correlation between the production temperature and the amount of chlorine produced by hydrogen, the application of sensors that can measure both the temperature and the hydrogen concentration is an important direction of development. Fiber optic gas sensors or ultrasound and semiconductor sensors may be able to measure the temperature and hydrogen concentration at the same time.

References

- 1 R. J. Kee, M. E. Coltrin, and H. Zhu: Chemically Reacting Flow: Theory, Modeling, and Simulation (John Wiley & Sons, New Jersey, 2018) 2nd ed., Chap. 2. <https://doi.org/10.1002/9781119186304>
- 2 Y. L. Liu, K. Thydén, M. Chen, and A. Hagen: Solid State Ionics **206** (2011) 97. <https://doi.org/10.1016/j.ssi.2011.10.020>
- 3 K. Hosoi and M. Ito: ECS Trans. **25** (2011) 67. <https://doi.org/10.1149/1.3205503>
- 4 S. Nagata, A. Momma, T. Kato, and Y. Kasuga: J. Power Sources **101** (2001) 60. [https://doi.org/10.1016/S0378-7753\(01\)00547-X](https://doi.org/10.1016/S0378-7753(01)00547-X)
- 5 Y. Zhang, J. H. Leu, A. Su, and T. S. Lan: Proc. 2021 IEEE 4th Int. Conf. Knowledge Innovation and Invention (IEEE, 2021) 13–18. <https://doi.org/10.1109/ICKII51822.2021.9574722>
- 6 T. Henriques, B. César, and P. J. C. Branco: Appl. Energy **87** (2009) 1400. <https://doi.org/10.1016/j.apenergy.2009.09.001>
- 7 Q. Zhao and F. C. Lee: IEEE Trans. Power Electron. **18** (2003) 65. <https://doi.org/10.1109/TPEL.2002.807188>
- 8 A. Su, Y. M. Ferng, C. B. Wang, and C. H. Cheng: Int. J. Energy Res. **37** (2013) 3071. <https://doi.org/10.1002/er.3071>
- 9 J. H. Leu, A. Su, S. C. Kuo, and K. C. Chen: Energies **17** (2024) 6083. <https://doi.org/10.3390/en17236083>
- 10 S. W. A. Shah, X. Jiang, Y. K. H. Li, G. Chen, J. Liu, Y. Gao, S. Zhang, and C. Pan: Appl. Therm. Eng. **258** (2025) 124560. <https://doi.org/10.1016/j.applthermaleng.2024.124560>
- 11 N. N. M. Tahir, N. A. Baharuddin, A. A. Samat, N. Osman, and M. R. Somalu: J. Alloys Compd. **894** (2022) 162458. <https://doi.org/10.1016/j.jallcom.2021.162458>
- 12 R. Peters, R. Deja, L. Blum, J. Pennanen, J. Kiviaho, and T. Hakala: Int. J. Hydrogen Energy **38** (2013) 6809. <https://doi.org/10.1016/j.ijhydene.2013.03.110>